Final Report
DOE Grant N. DE-FG05-08OR23337

Quantum Monte Carlo Endstation for Petascale Computing

North Carolina State U. PI: Prof. Lubos Mitas
Department of Physics and Center for High Performance Simulations
North Carolina State University (NCSU), Raleigh, NC, 27695-8202
Email: lmitas@unity.ncsu.edu
December 21, 2010

Project Lead

This project was led by Prof. David M. Ceperley, University of Illinois at Urbana-Champaign, who coordinated the work of the involved research groups (ORNL, UIUC, NCSU, College of William and Mary, Cornell U., Florida State U.) The work was coordinated through regular skype and conference calls and during meetings of the research groups and PIs at several conferences and workshops. Also for the exchange of data, codes, files, written notes and records, a Wiki webpage was established on a server at U. of Illinois and it was very actively used during the project period.

1 Summary of Accomplishments at NCSU, PI: L. Mitas

NCSU research group has been focused on accomplising the key goals of this initiative: establishing new generation of quantum Monte Carlo (QMC) computational tools as a part of Endstation petaflop initiative for use at the DOE ORNL computational facilities and for use by computational electronic structure community at large; carrying out high accuracy quantum Monte Carlo demonstration projects in application of these tools to the forefront electronic structure problems in molecular and solid systems; expanding the impact of QMC methods and approaches; explaining and enhancing the impact of these advanced computational approaches.

In particular, we have developed quantum Monte Carlo code (**QWalk, www.qwalk.org**) which was significantly expanded and optimized using funds from this support and **at present became an actively used tool in the petascale regime by ORNL researchers and beyond**. These developments have been built upon efforts undertaken by the PI's group and collaborators over the period of the last decade. The code was optimized and tested extensively on a number of parallel architectures including petaflop ORNL Jaguar machine. We have developed and redesigned a number of code modules such as evaluation of wave functions and orbitals, calculations of pfaffians and introduction of backflow coordinates together with overall organization of the code and random walker distribution over multicore architectures. We have addressed several bottlenecks such as load balancing and verified efficiency and accuracy of the calculations with the other groups of the Endstation team. **The QWalk package contains about 50,000 lines of high quality object-oriented C++ and includes also interfaces to data files from other conventional electronic structure codes** such as Gamess, Gaussian, Crystal and others.

This grant supported PI for one month during summers, a full-time postdoc and partially three graduate students over the period of the grant duration, it has resulted in 13 published papers, 15 invited talks and lectures nationally and internationally. My former graduate student and **postdoc Dr. Michal Bajdich, who was supported byt this grant, is currently a postdoc with ORNL in the group of Dr. F. Reboredo and Dr. P. Kent and is using the developed tools in a number of DOE projects**. The QWalk package has become a truly important research tool used by the electronic structure community and has attracted several new developers in other research groups.

Our tools use several types of correlated wavefunction approaches, variational, diffusion and reptation methods, large-scale optimization methods for wavefunctions and enables to calculate energy differences such as cohesion, electronic gaps, but also densities and other properties, using multiple runs one can obtain equations of state for given structures and beyond. Our codes use efficient numerical and Monte Carlo strategies (high accuracy numerical orbitals, multi-reference wave functions, highly accurate correlation factors, pairing orbitals, force biased and correlated sampling Monte Carlo, are robustly parallelized and enable to run on tens of thousands cores very efficiently.

Our demonstration applications were focused on the challenging research problems in several fields of materials science such as transition metal solids. We note that **our study of FeO solid was the first QMC calculation of transition metal oxides at high pressures**.

2 Papers.

We have produced 13 papers from which one was published in Phys. Rev. Lett. Two of the papers are long reviews of 87 and 55 pages, Refs. [5] and [13], respectively. Ref. [6] describes the developed QWalk tools, with further details left to the website www.qwalk.org. Ref. [4] described the overall effort of the Endstation project with contributions from all research groups involved. Several of the papers appeared in 2010 due to the usual process of reviewing and responses to referees comments and suggestions and resubmitting new versions.

- [13] J. Kolorenc and L. Mitas, "Applications of quantum Monte Carlo in condensed systems", Reports on Progress in Physics, accepted, in press.
- [12] J. Kolorenc, S. Hu and L. Mitas, "Wave functions for quantum Monte Carlo calculations in solids: Orbitals from density functional theory with hybrid exchange-correlation functionals", Phys. Rev. B, p. 115108, vol. 82, (2010).
- [11] J. Kolorenc, L. Mitas, Electronic structure of solid FeO at high pressures by quantum Monte Carlo, Physics Procedia 3, 1437-1441 (2010)
- [10] M. Bajdich, J. Kolorenc, L. Mitas, and P. J. Reynolds, Pairing in Cold Atoms and other Applications for Quantum Monte Carlo methods, Physics Procedia 3, 1397-1410 (2010)
- [9] L. Mitas, J. Kolorenc, Quantum Monte Carlo Studies of Transition Metal Oxides, Reviews in Mineralogy and Geochemistry, 71, 137, (2010).
- [8] W.A. Lester, Jr., L. Mitas, B.L. Hammond, Quantum Monte Carlo for atoms, molecules and solids (invited review), Chem. Phys. Lett. 478, 1 (2009).
- [7] H. Kino, L.K. Wagner, L. Mitas, Theoretical study of electronic and atomic structures of (MnO)n, J. of Computational and Theoretical Nanoscience, 6, 2583 (2009).
- [6] L.K. Wagner, M. Bajdich, L. Mitas, QWalk: quantum Monte Carlo code for electronic structure, J. Comput. Phys., 228, 3390 (2009).
- [5] M. Bajdich, L. Mitas, Electronic structure quantum Monte Carlo, Acta Physica Slovaca, 59, 81-168 (2009)
- [4] K.P. Esler, J. Kim, D.M. Ceperley, W. Purawanto, E.J. Walter, H. Krakauer, S. Zhang, P.R.C. Kent, R.G. Hennig, C. Umrigar, M. Bajdich, J. Kolorenc, L. Mitas, A. Srinivasan, Quantum Monte Carlo algorithms for electronic structure at the petascale; the Endstation project, Journal of Physics: Conference Series 125 012057: 1-15 (2008).
- [3] J. Kolorenc, L. Mitas, Quantum Monte Carlo calculations of structural properties of FeO solid under pressure, Phys. Rev. Lett. 101, 185502 (2008); cond-mat/0712.3610

- [2] M. Bajdich, L. Mitas, K.E. Schmidt, Pfaffian pairing and backflow wavefunctions for electronic structure quantum Monte Carlo methods, Phys. Rev. B 77, 115112 (2008); cond-mat/0610088.
- [1] L. Mitas, M. Bajdich, Nodal properties of fermion wave functions, in Recent Progress in Many-Body Theories XIV, Ed. J. Boronat, G. E. Astrakharchik, F. Mazzanti, World Scientific, New Jersey, 2008, pp.193-203.

3 Invited talks.

- Two colloquia for graduate students at MIT, BU and Harvard U., Boston, MA, Dec. 2009
- Excited States In Density Functional Theory Workshop, Kavli Institute of Theoretical Physics, UC Santa Barbara, Oct. 2009
- Excited states in condensed matter Workshop, Kavli Institute, UC Santa Barbara, Oct. 2009
- International Workshop on Many-Body Methods for Strongly Correlated Systems, Leiden, Netherlands, August 2009
- Many-Body Methods for Correlated Electrons Workshop, ORNL, April 2009
- Current advances in quantm Monte Carlo, ACS Meeting, Salt Lake City , March 2009
- FeO solid at high pressures: quantum Monte Carlo study, invited talk at workshop on strongly correlated systems, Oak Ridge National Laboratory, Nov. 2008
- Current advances in quantm Monte Carlo, Seminar at Center for Integration of Nanomaterial Systems, UC Berkeley, Sep. 2008
- Topology of fermion wavefunctions, Summer school and workshop, Aspen, CO, August 2008
- Quantum Monte Carlo methods, International Symposium, Vancouver, July 2008
- Quantum Monte Carlo: fermion nodes and pfaffian pairing wavefunctions, International Symposium, Tokyo, June 2008
- Topology of fermion wavefunctions, Quantum Simulations and Design, International Workshop, Tokyo, May 2008
- Quantum Monte Carlo Methods, Seminar, Brookhaven National laboratory, Long Island, May 2008
- Quantum Monte Carlo Methods, Seminar, Pennsylvania State University, Pennsylvania, April 2008
- Topology of fermion nodes and pfaffian pairing wavefunctions, Sanibel theoretical and computational quantum chemistry meeting, Georgia, February 2008

2 more invited talks were given by the postdoc M. Bajdich in 2009.

4 Quantum Monte Carlo computational tools: QWalk.

In what follows we describe several aspects of QWalk, a computational package capable of performing QMC electronic structure calculations for molecules and solids with many electrons. We outline the structure of the program and its implementation of Quantum Monte Carlo methods. It is open-source, licensed under the GPL, and available at the web site http://www.qwalk.org.

4.1 Challenge of accurate electronic structure calculations.

For many problems in chemistry and solid-state physics, we are interested in solving for the eigenstates of the electronic Born-Oppenheimer Hamiltonian

$$H = -\frac{1}{2}\sum_i \nabla_i^2 - \sum_{iI} \frac{Z_I}{r_{iI}} + \sum_{i>j} \frac{1}{r_{ij}}, \tag{1}$$

where upper/lower cases indicate nuclei/electrons. This problem is very challenging because the wave function is a general function in $3N_e$-dimensional space (where N_e is the number of electrons), which the Coulomb interaction guarantees is not separable into a product of 3-dimensional functions. Over the past six decades or so, physicists and chemists have generated many powerful approximations and theories that attempt to solve the electronic structure problem to varying degrees of accuracy. Among these are the successful Hartree-Fock (HF), post Hartree-Fock (post-HF), and Density Functional theories (DFT). Each of these methods occupies its place in the computational toolbox. DFT is a good tradeoff between accuracy and computational efficiency, allowing thousands of electrons to be treated, usually getting qualitative trends correct for most quantities(such as band gaps, cohesive/binding energies, and other energy differences between different systems), and is often quantitatively correct for some quantities (such as geometries). To treat the quantum many-body problem more accurately, one can turn to post-Hartree-Fock methods, which are often quantitatively correct; however, they scale quite poorly with the system size (approximately $\mathrm{O}(N_e^{5-7})$). There are few methods that both scale well, at most $\mathrm{O}(N_e^3)$, and also offer higher accuracy than DFT.

Quantum Monte Carlo methods fill this gap by using stochastic algorithms to treat the many-body wave function in the full $3N_e$-dimensional space. It has several advantages–good scaling in the number of electrons ($\mathrm{O}(N_e^{0-3})$) and is easily implemented in parallel at 99% efficiency. Over the past $\sim$20 years, QMC has been applied to a host of systems including atoms, molecules, clusters, surfaces and solids, with impressive accuracy across this wide range.

QMC methodology has proved to be a powerful technique for studies of quantum many-body systems and also real materials. In essence, QMC has a number of advantages when compared with other approaches:

- direct and explicit many-body wave function framework for solving the stationary Schrödinger equation;
- favorable scaling with the systems size;
- wide range of applicability;
- the fixed-node approximation which enables to obtain 90-95% of the correlation effects;
- scalability on parallel machines;
- new insights into the many-body phenomena.

For extended systems, particularly, it is the most accurate method available for total energies on the materials that have been tested. However, there are very few programs available that perform these calculations. We have developed a new program QWalk for general purpose QMC calculations written in C++ with modern programming techniques and incorporating state of the art algorithms in a fast and scalable code. QWalk has already been used in a number of publications and in what follows we present an overview of its structure and capabilities.

5 Methods

5.1 Variational Monte Carlo

The expectation value for an arbitrary operator $\mathcal{O}$ and a given trial variational wave function Ψ_T is given by

$$\langle \mathcal{O} \rangle = \frac{\langle \Psi_T | \mathcal{O} | \Psi_T \rangle}{\langle \Psi_T | \Psi_T \rangle} = \frac{\int \Psi_T^2(\mathbf{R}) [\mathcal{O}\Psi_T(\mathbf{R})/\Psi_T(\mathbf{R})] d\mathbf{R}}{\int \Psi_T^2(\mathbf{R}) d\mathbf{R}}$$

where $\mathbf{R} = (\mathbf{r}_1, \mathbf{r}_2, ..., \mathbf{r}_{N_e})$ denotes a set of N_e electron coordinates in 3D space. Typically, such integrals are evaluated by reducing the multi-dimensional integral into a sum of products of low-dimensional integrals. Unfortunately, this either restricts the functional form of $\Psi_T(R)$ or makes the calculations undoable for more than a few electrons. One of the key motivations for employing stochastic approaches is to eliminate this restriction and to gain qualitatively new variational freedom for describing many-body effects.

In order to evaluate the expectation value integral stochastically we first generate a set $\{\mathbf{R}_m\}$ of statistically independent sampling points distributed according to $\Psi_T^2(\mathbf{R})$ using the Metropolis algorithm. The expectation value is then estimated by averaging over the samples $\{\mathbf{R}_m\}$. For example, the VMC energy is given by the average of the quantity called local energy

$$\begin{aligned} E_{VMC} &= \frac{1}{M} \sum_{m=1}^{M} \frac{H\Psi_T(\mathbf{R}_m)}{\Psi_T(\mathbf{R}_m)} + \varepsilon \\ &= \frac{1}{M} \sum_{m=1}^{M} E_{loc}(\mathbf{R}_m) + \varepsilon \end{aligned}$$

with the statistical error ε proportional to $1/\sqrt{M}$.

It is straightforward to apply the variational theorem in this framework. Consider a variational wave function $\Psi_T(R, P)$, where R is the set of all the electron positions and P is the set of variational parameters in the wavefunction

$$E(P) = \frac{\int \Psi_T(\mathbf{R}, P) H \Psi_T(\mathbf{R}, P) d\mathbf{R}}{\int \Psi_T^2(\mathbf{R}, P) d\mathbf{R}} \tag{2}$$

A (hopefully) good approximation to the ground state is then the wavefunction with the set of parameters P that minimizes $E(P)$. The stochastic method of integration allows us to use explicitly correlated trial wave functions such as the Slater-Jastrow form, along with other functional forms as explained later. In fact, as long as the trial function and its derivatives can be evaluated quickly, any functional form can be used.

Within the program, this procedure is broken down into two parts: sampling Ψ_T^2 while evaluating energy and other properties, and optimizing the wave function. The first part, sampling Ψ_T^2, is carried out using the Metropolis-Hastings algorithm. We start with a point $\mathbf{R}$ in $3N_e$ dimensional space and generate a second point $\mathbf{R}'$ according to the transition probability $T(\mathbf{R}' \leftarrow \mathbf{R})$. T is a completely arbitrary function so long as $T(\mathbf{R}' \leftarrow \mathbf{R}) \neq 0 \Leftrightarrow T(\mathbf{R} \leftarrow \mathbf{R}') \neq 0$; that is, all moves are reversible. We then accept the move with probability

$$a = min\left(1, \frac{\Psi_T^2(\mathbf{R}') T(\mathbf{R}' \leftarrow \mathbf{R})}{\Psi_T^2(\mathbf{R}) T(\mathbf{R} \leftarrow \mathbf{R}')}\right). \tag{3}$$

After a few steps, the distribution converges to Ψ_T^2, and we continue making the moves until the statistical uncertainties are small enough. The total energy and its components are evaluated, as well as other properties.

We then optimize the wave function using a fixed set of sample points. Since the samples are then correlated, small energy differences can be determined with much greater precision than the total energy. There are many quantities other than energy that, upon being minimized, will provide a good

approximation to the ground state wave function. One important one is the variance of the local energy; that is

$$\sigma^2 = \frac{\int d\mathbf{R}\Psi_T^2(\mathbf{R})(E_{loc} - \langle E_{loc}\rangle)^2}{\int d\mathbf{R}\Psi_T^2(\mathbf{R})}. \tag{4}$$

Since E_{loc} is a constant when $|\Psi_T\rangle = |\Phi_0\rangle$, the variance will go to zero for an exact eigenstate. There are several other possible functions, listed in Sec 7.2, but variance and energy are the most common quantities to minimize.

5.2 Projector Monte Carlo

To obtain accuracy beyond a given ansatz, we employ another method which projects out the ground state of a given symmetry from any trial wave function. To do this, we simulate the action of the operator $e^{-(H-E_0)\tau}$ on the trial function, where τ is the projection time and E_0 is the self-consistently determined energy of the ground state. As $\tau \to \infty$, $e^{-(H-E_0)\tau}\Psi_T \to \Phi_0$, where Φ_0 is the ground state. For large τ, there is no general expansion for $e^{-(H-E_0)\tau}$, but for small τ, we can write the projection operator in $\mathbf{R}$-representation as

$$\begin{aligned} G(\mathbf{R}', \mathbf{R}, \tau) \simeq & \, exp(-(\mathbf{R}' - \mathbf{R})^2/2\tau) \\ & \times exp(-\tau(V(\mathbf{R}) + V(\mathbf{R}') - 2E_0)/2) \end{aligned}$$

which can be interpreted as a dynamic diffusion kernel $G_D(\mathbf{R}', \mathbf{R}, \tau) = exp(-(\mathbf{R}' - \mathbf{R})^2/2\tau)$ while the other term represents the branching kernel $G_B(\mathbf{R}', \mathbf{R}, \tau) = exp(-\tau(V(\mathbf{R}) + V(\mathbf{R}') - 2E_0)/2)$.

The basic idea of projector Monte Carlo is to sample a path $G(\mathbf{R}_N, \mathbf{R}_{N-1}, \tau)...G(\mathbf{R}_2, \mathbf{R}_1, \tau)\Psi_T(\mathbf{R}_1)$. For N large enough (for a long enough path), the distribution of $\mathbf{R}_N$ will approach Φ_0. However, to interpret this as a stochastic process, the path distribution must be positive; that is, the product of all G's with Ψ_T must be positive. This gives rise to the fixed node approximation, where the nodes (the places where the trial function equals zero) of the trial wave function are approximated as the nodes of the ground state wave function. One can avoid this restriction by performing a released-node calculation although the price is a change from polynomial to exponential scaling with system size. With the nodal constraint, the projector Monte Carlo approach typically obtains 90-95% of the correlation energy in an amount of time proportional to a low order polynomial(2-3) of the system size.

In actual calculations, we perform an importance-sampling transformation, where $G(\mathbf{R}', \mathbf{R}, \tau)$ is replaced by the importance sampled Green's function

$$\tilde{G}(\mathbf{R}', \mathbf{R}, \tau) = \Psi_T(\mathbf{R}')G(\mathbf{R}', \mathbf{R}, \tau)/\Psi_T(\mathbf{R}) \tag{5}$$

The dynamic part of the Green's function then becomes

$$G_D(\mathbf{R}', \mathbf{R}, \tau) = exp(-(\mathbf{R}' - \mathbf{R} - \tau\nabla ln\Psi_T(\mathbf{R}))^2/2\tau) \tag{6}$$

and the branching part becomes

$$G_B(\mathbf{R}', \mathbf{R}, \tau) = exp(-\tau(E_L(\mathbf{R}) + E_L(\mathbf{R}') - 2E_0)/2), \tag{7}$$

both of which are much better-behaved stochastically, since the 'force' $\nabla ln\Psi_T(\mathbf{R})$ biases the walk to where the wavefunction is large, and the local energy $E_L(\mathbf{R})$ is much smoother than the potential energy. Then if we generate the path $\tilde{G}(\mathbf{R}_N, \mathbf{R}_{N-1}, \tau)...\tilde{G}(\mathbf{R}_2, \mathbf{R}_1, \tau)\Psi_T^2(\mathbf{R}_1)$, for large enough N, the distribution of $\mathbf{R}_N$ is $\Psi_T(\mathbf{R}_N)\Phi_0(\mathbf{R}_N)$, which is called the mixed distribution. The ground state energy is obtainable by evaluating the integral $\int \Psi_T\Phi_0 H\Psi_T/\Psi_T d\mathbf{R} = \int \Phi_0 H\Psi_T d\mathbf{R} = E_0$, since Φ_0 is an eigenstate of H within the nodal boundaries. In QWalk, two versions of the projector method are implemented: Diffusion Monte Carlo, which has the advantage that the large N limit is easily obtained, and Reptation Monte Carlo, which makes the 'pure' distribution Φ_0^2 available.

Diffusion Monte Carlo has been discussed by many authors, and suffice it to say that it attains the mixed distribution by starting with a distribution of Ψ_T^2 and interpreting the action of the Green's function as a

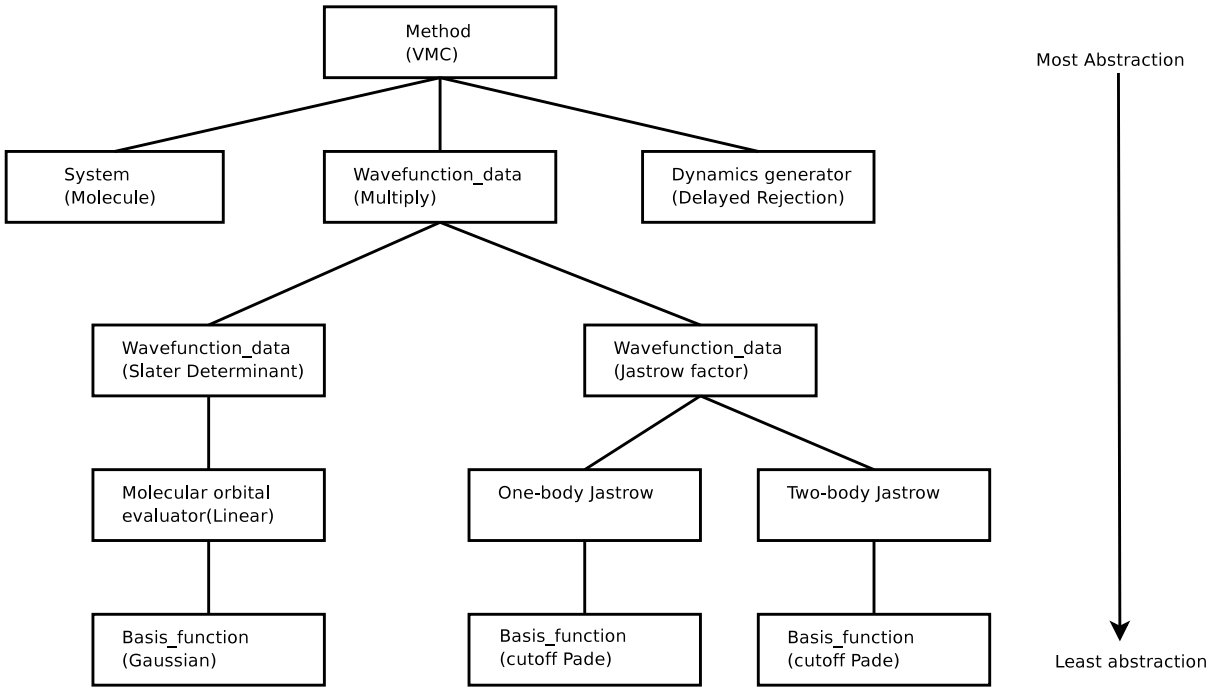

Figure 1: Calculation structure for the VMC method on a molecule using a Slater-Jastrow wave function.

stochastic process with killing and branching, eventually ending up with $\Psi_T\Phi_0$. It has the advantage that the $\tau \to \infty$ limit is easy to achieve, but the disadvantage of not having access to the pure distribution. A more subtle limitation is that the branching process spoils any imaginary-time data and can decrease the efficiency of the simulation if there is too much branching. Even with these limitations, DMC is probably the most efficient way to obtain the fixed-node approximation to the ground state energy.

For quantities that do not commute with the Hamiltonian, we use Reptation Monte Carlo with the bounce algorithm. We sample the path distribution

$$\Pi(s) = \Psi_T(\mathbf{R}_0)G(\mathbf{R}_0, R_1, \tau)\ldots G(\mathbf{R}_{n-1}, \mathbf{R}_n, \tau)\Psi_T(\mathbf{R}_n) \tag{8}$$

where $s = [\mathbf{R}_0, \mathbf{R}_1, \ldots, \mathbf{R}_{n-1}, \mathbf{R}_n]$ is a projection path. In the limit as $\tau \to \infty$, $exp(-H\tau)|\Psi_T\rangle \to |\Phi_0\rangle$, the ground state, and, since it is a Hermitian operator, the conjugate equation also holds. Therefore, the distribution of $\mathbf{R}_0$ and $\mathbf{R}_n$ is the mixed distribution $\Psi_T(\mathbf{R})\Phi_0(\mathbf{R})$,and the distribution of $\mathbf{R}_{n/2}$ is $\Phi_0^2(\mathbf{R}_{n/2})$ in the limit as $n \to \infty$. We evaluate the energy as $E_{RMC} = \langle[E_L(\mathbf{R}_0) + E_L(\mathbf{R}_N)]/2\rangle$ and operators non-commuting with H as $O_{RMC} = \langle O(\mathbf{R}_{N/2})\rangle$ Reptation Monte Carlo does not include branching, instead using an acceptance/rejection step. This is a tradeoff, allowing us to project only for a finite τ, since otherwise the probability distribution function is not normalizable, but allowing access to the pure distribution and imaginary time correlations. The path can sometimes get stuck, however, even with the bounce algorithm, which limits the efficiency of the algorithm. In QWalk, RMC is approximately as efficient as DMC until the rejection rate begins to increase, making the path move very slowly. In our calculations, this slowdown appears at approximately 150 electrons.

6 Organization and Code Structure

The code is written in a combination of object-oriented and procedural techniques. The object-oriented approach is coarse-grained, creating independent sections of code that are written efficiently in a procedural fashion. It is extremely modular; almost every piece can be removed and replaced with

Table 1: The central objects of the code and their physical correspondents

Module name	**Mathematical object**
System	parameters and form of the Hamiltonian
Sample point	$\mathbf{R}$, the integration variables
Wave function type	Wave function ansatz
Wave function	$\Psi_T(\mathbf{R})$, $\nabla\Psi_T(\mathbf{R})$, $\nabla^2\Psi_T(\mathbf{R})$
Dynamics generator	Metropolis trial move (Green's function)

another. A contributor of a module only has to change one line in the main code to allow use of a new module. This allows for flexibility while keeping the code base relatively simple and separable. The modular structure also allows for partial rewrites of the code without worrying about other parts. In fact, each major module has been rewritten several times in this manner as we add new features and refactor the code. For the user, this structure shows itself in flexibility.

The modules form a tree of successive abstractions (Fig 1). At the top of the tree is the QMC method, VMC in this case. It works only in terms of the objects directly below it, which are the concepts of System, Wave function data, etc. (see Table 1). These in turn may have further abstractions below them, as we've shown for the wave function object. The highest wave function object is of type 'Multiply', which uses two wave function types to create a combined wave function. In this case, it multiplies a Slater determinant with a Jastrow correlation factor to form a Slater-Jastrow function. Since the wave functions are pluggable, the Slater determinant can be replaced with any antisymmetric function, as well as the Jastrow factor. The type is listed along with the specific instant of that type in parenthesis. At each level, the part in parenthesis could be replaced with another module of the same type.

We present an implementation of the VMC algorithm as an example of how the code is organized(Fig 2). For reasons of space, we do not write the function line-by-line, which includes monitoring variables, etc., but instead give a sketch of the algorithm. The VMC method works at the highest level of abstraction, only in terms of the wave function, system, and random dynamics. It does not care what kind of system, wave function, etc. are plugged in, only that they conform to the proper interfaces.

We will now provide a listing of the available modules for the major types, along with some details of their implementation.

7 Methods Implementation

7.1 Variational Monte Carlo

The VMC module implements the Metropolis method to sample the probability density $\Psi_T^2(\mathbf{R})$. It has been described in Sec 5.1 to some detail–the method is more or less a direct translation. Beyond the basic algorithm, it implements correlated sampling as explained in Sec 7.5 for small energy differences between very similar systems.

7.2 Optimization of Wave Functions

We have implemented three different methods for optimization. All methods are capable of optimizing several objective functions (See Table 2). Any of these objective functions will obtain the correct ground state with an infinitely flexible function, but may obtain different minima for incomplete wave functions and some are easier to optimize than others. The first (OPTIMIZE) is based on variance optimization. The method minimizes the objective function on a set of fixed configurations from VMC using a conjugate gradient technique, usually not reweighting the averages as the wave function changes. Optimizing the energy using OPTIMIZE is quite expensive, because it requires many configurations to evaluate an

```
Vmc_method::run(vector <string> & vmc_section,
                vector <string> & system_section,
                vector <string> & wavefunction_section) {

  //Allocate the objects we will be working with
  System * sys=NULL;
  allocate(sys, system_section);

  Wavefunction_data * wfdata=NULL;
  allocate(wfdata, sys, wavefunction_section);

  Sample_point * sample=NULL;
  sys->generateSample(sample);
  Wavefunction * wf=NULL;
  wfdata->generateWavefunction(wf);

  //the Sample_point will tell the Wavefunction
  //when we move an electron
  sample->attachWavefunction(wf);
  sample->randomGuess();

  //This is the core part of the VMC algorithm
  for(int s=0; s< nsteps; s++) {
    for(int e=0; e < nelectrons; e++) {
       dynamics_generator->sample(e,timestep,wf,sample);
    } //end electron loop
    //gather averages
  } //end step loop

  //report final averages
```

Figure 2: Sketch of the main loops in a simplified code for the VMC method

unbiased estimate of the energy derivative.

Method OPTIMIZE2 also uses a fixed set of configurations, but instead of evaluating only the first derivatives of the objective function, as conjugate gradients do, it uses a low-variance estimator for the Hessian matrix and Newton's method to find the zeros of the first derivatives. OPTIMIZE2 is able to produce better wave functions with lower energies than OPTIMIZE by directly optimizing the energy even for very large systems (we have applied it for up to 320 electrons) while costing slightly more.

Finally, NEWTON_OPT uses a fixed set of configurations to evaluate only a single Hessian matrix, then evaluates the optimal length of the optimization step using VMC correlated sampling, as suggested by another U. Cornell group lead C. Umrigar. This method is able to find the very lowest energy wave functions, since the configurations are regenerated every optimization step. However, NEWTON_OPT is much more expensive than the other two methods.

Table 2: Optimization objective functions implemented

Function	**Minimized quantity**
Variance	$\langle (E_L(\mathbf{R}) - E_{ref})^2 \rangle$
Absolute value	$\langle \lvert E_L(\mathbf{R}) - E_{ref} \rvert \rangle$
Lorentz	$\langle ln(1 + (E_L(\mathbf{R}) - E_{ref})^2/2) \rangle$
Energy	$\langle E_L(\mathbf{R}) \rangle$
Mixed	$aEnergy + (1-a)Variance, 0 < a < 1$

7.3 Diffusion Monte Carlo

DMC is implemented almost identically to VMC, except that the time step is typically much smaller and each walker accumulates a weight equal to $\exp(-\frac{\tau_{eff}}{2}(E_L(\mathbf{R}') + E_L(\mathbf{R}) - 2E_{ref}))$. Since we use an acceptance/rejection step, τ_{eff} is chosen somewhat smaller than τ as $\tau_{eff} = p\tau$, where p is the acceptance ratio. To control the fluctuations in the weights, we employ a constant-walker branching algorithm, which improves the parallel load balancing properties of DMC. Every few steps we choose a set of walkers that have large weights (w_1) for branching. Each one of these walkers is matched with a smaller weight walker (w_2) which is due for killing. The large weight walker is branched and the small weight walker is killed with probability $\frac{w_1}{w_1+w_2}$, with each copy gaining a weight of $\frac{w_1+w_2}{2}$. Otherwise, the small weight walker is branched and the large weight walker is killed, with the copies having the same weight as before. Walkers are then exchanged between nodes to keep the number of walkers on each node constant, and thus preserve high parallel efficiency. QWalk keeps track of two numbers: E_{ref} and E_0. E_{ref} is first set to the VMC average energy, and then to the energy of the last block. The energy that goes into the weights, E_0, is then calculated every few steps as

$$E_0 = E_{ref} - log\left(\frac{\sum w_i}{N_{conf}}\right), \tag{9}$$

where N_{conf} is the number of sample points (configurations) in the simulation.

During the DMC calculation, the local energy will very occasionally fluctuate down drastically, causing the weight to increase too much. This can be fixed by cutting off the weights. For fluctuations beyond ten standard deviations of the energy, we smoothly bring the effective time step to zero for the weights, which avoids the efficiency problem without introducing a noticeable error.

7.4 Reptation Monte Carlo

The fluctuations in the local energy part of the Green's function can cause the path in RMC to get stuck, so we cut off the effective time step in the same way as in DMC. The branching part of the Green's function is otherwise quite smooth. We use the same dynamic Green's function as we do in DMC (either a standard metropolis rejection step or the UNR algorithm), so we accept/reject based only on the branching part of the Green's function. We use the bounce algorithm, which improves the efficiency by allowing the path to explore the many-body phase space much more quickly.

7.5 Correlated Sampling

Correlated sampling is a technique where one samples two very similar systems with the same sets of samples. The variance in the difference will decrease as $Var(X-Y) = Var(X) + Var(Y) - 2Cov(X,Y)$, so for perfectly correlated sampling, the variance will be zero for the difference. In QWalk, this is handled by performing a primary walk that samples some probability distribution $P_1(X)$. Averages are obtained as usual by calculating the integral $\langle O_1 \rangle = \int P_1(X) O_1 dX$. Suppose we wish to find $\langle O_2 - O_1 \rangle$. It can be written as

$$\int P_2(X)O_2 - P_1(X)O_1 dX = \int P_1(X)\left[\frac{P_2}{P_1}O_2 - O_1\right] dX. \tag{10}$$

Since we are sampling $P_1(X)$, in the Monte Carlo averaging, this integral is evaluated by averaging the weighted difference over sample points:

$$\sum_i^N \left[\frac{w_i(X_i)O_2(X_i)}{\sum_j w_i(X_i)} - \frac{O_1(X_i)}{N}\right] \tag{11}$$

The difference in the methods is only in how they determine the weights.

VMC, DMC and RMC all support correlated sampling between arbitrary systems. In VMC, the weights are $w(X) = \frac{\Psi_2^2(X)}{\Psi_1^2(X)}$, which is an exact relationship. DMC and RMC both require some approximation to the Green's function to weight the secondary averages properly.

8 Systems

8.1 Boundary Conditions

Most systems of interest are treatable either by open boundary conditions or periodic boundary conditions. Adding new boundary conditions is also quite simple. Molecules with arbitrary atoms, charge, spin state, and with finite electric field are supported. In 3D periodic systems, the calculation can be done at any real k-point, allowing k-point integrations (recently, complex points were implemiented as well). In many-body simulations, there is an additional finite size approximation due to the Coulomb interaction between image electrons. We correct this as $\delta E = \frac{c}{r_s}$, where the r_s is that of the homogeneous electron gas and c has been empirically fitted to 0.36 Hartrees. We have found this correction to function about as well as other methodologies to correct the finite size error. The code has been used on systems with up to 135 atoms and 1080 electrons; the limiting factor is the amount of computer time needed to reduce the stochastic uncertainties.

8.2 Pseudopotentials

QWalk accepts pseudopotentials as an expansion of nonlocal angular momentum operators:

$$\hat{V}_{ECP} = V_{local}(\mathbf{R}) + \sum_{l=0}^{lmax} V_l(\mathbf{R})|l\rangle\langle l| \tag{12}$$

for arbitrary maximum angular moment. V_l is a basis function object that is typically a spline interpolation of a grid or a sum of Gaussian functions. While any pseudopotential of this form can be used, we use soft potentials in which the $\frac{Z}{r}$ divergence has been removed from the nuclei-electron interaction. These potentials have been created specifically for QMC and are available in the literature although more traditional Hartree-Fock or DFT pseudopotentials in the Troullier-Martins form work as well.

9 Forms of the Wave function

For Coulomb interactions systems, the first-order trial function is usually written as a Slater determinant taken from Hartree-Fock or Density Functional Theory multiplied by a correlation factor(known as a Jastrow factor) which is optimized in Variational Monte Carlo. Between 90% and 95% of the correlation energy is typically obtained with this trial wave function in Diffusion Monte Carlo.

One of the attractions of QMC is that, since all the integrals are done by Monte Carlo, almost any ansatz can be used, as long as it is reasonably quick to evaluate. QWalk's modular structure makes adding new wave function forms as simple as coding one-electron updates of the function value and derivatives, and adding one line to the main code to support loading of the module. We have implemented several forms of wave functions, which the user can combine. For example, to create the Slater-Jastrow wave function, the user first asks for a multiply object, which contains two wave function objects. The user then fills in a Slater determinant object and a Jastrow object. For a Pfaffian-Jastrow wave function, the user replaces the Slater determinant input with the Pfaffian input. Obviously, it is up to the user to make sure that the total wave function is properly antisymmetric and represents the problem correctly.

9.1 Slater Determinant(s)

This is the standard sum of Slater determinants, written as $\Psi_T = \sum c_i D_i^{\uparrow} D_i^{\downarrow}$, where $D_i^{\uparrow(\downarrow)}$ is a determinant of the spin up(down) one-particle orbitals. The coefficients are optionally optimizable within VMC.

9.2 Jastrow Factor

The Jastrow factor is written as e^U, where

$$U = \sum_{iIk} c_k^{ei} a_k(r_{iI}) + \sum_{ijk} c_k^{ee} b_k(r_{ij}) + \sum_{ijIklm} c_{klm}^{eei}[a_k(r_{iI})a_l(r_{jI}) + a_k(r_{jI})a_l(r_{iI})]b_m(r_{ij}), \tag{13}$$

i, j are electron indices, and I is a nuclear index. Both the coefficients and parameters within the basis functions can be optimized. For the basis functions, we satisfy the exact electron-electron cusp conditions with the function $b(r) = cp(r/rcut)/(1 + \gamma p(r/rcut))$, where $p(z) = z - z^2 + z^3/3$, γ is the curvature, which is optimized, and c is the cusp(0.25 for like spins and 0.50 for unlike spins). Further correlation is added by including functions of the form $b_k(r) = a_k(r) = \frac{1-zpp(r/rcut)}{1+\beta zpp(r/rcut)}$ where $zpp(x) = x^2(6 - 8x + 3x^2)$ and β is an optimized parameter. These functions have several favorable properties, going smoothly to zero at a finite cutoff radius, and covering the entire functional space between 0 and $rcut$. This allows the Jastrow factor to be extremely compact, typically requiring optimization of around 25 parameters while still coming close to saturating the functional form. While these are the standard basis functions, they can be replaced or augmented by any in the program by a simple change to the Jastrow input. The third term in Eqn 13, which sums over two electron indices and ionic indices, can be expensive to evaluate for large systems and is sometimes excluded. A Jastrow factor with only the first two terms is called a two-body Jastrow, and with the eei term included is called a three-body Jastrow.

9.3 Pfaffian Pairing Wave Function

We write the wave function as $\Psi_T = e^U det\Phi$, where e^U is the Jastrow factor of above and the matrix $\Phi_{ij} = \chi(r_i, r_j)$ is the pairing function between opposite-spin electrons(the function is easily extended for $N_{up} \neq N_{down}$). This function contains the Slater determinant as a special case when χ is written as the sum over the occupied single-particle orbitals: $\chi(r_i, r_j) = \sum_k^{N_e} \phi_k(r_i)\phi_k(r_j)$. We have implemented the Pfaffian pairing wave function, which allows not only unlike-spin pairing, as the canonical projection of the BCS wave function does, but also allows like-spin pairing. The wave function is written as the Pfaffian of the matrix P, appears as the following:

$$P = \mathrm{pf} \begin{bmatrix} \boldsymbol{\xi}^{\uparrow\uparrow} & \boldsymbol{\Phi}^{\uparrow\downarrow} & \boldsymbol{\varphi}^{\uparrow} \\ -\boldsymbol{\Phi}^{\uparrow\downarrow T} & \boldsymbol{\xi}^{\downarrow\downarrow} & \boldsymbol{\varphi}^{\downarrow} \\ -\boldsymbol{\varphi}^{\uparrow T} & -\boldsymbol{\varphi}^{\downarrow T} & 0 \end{bmatrix}. \tag{14}$$

The Φ matrices are the same as in the BCS wave function, and the φ matrices are made up of the one-particle orbitals for a spin-polarized system. The $\boldsymbol{\xi}$ are antisymmetric triplet pairing matrices. The operation of the Pfaffian ensures that the entire wave function is antisymmetric. The Pfaffian wave function contains the BCS wave function as a special case without triplet pairing, and thus contains the Slater determinant wave function as well. The general expansion for Φ is

$$\Phi(\mathbf{r}_1, \mathbf{r}_2) = \sum_{kl} c_{kl}\phi_k(\mathbf{r}_1)\phi_l(\mathbf{r}_2) \tag{15}$$

under the constraint that $c_{kl} = c_{lk}$. $\boldsymbol{\xi}$ is written in a very similar way:

$$\boldsymbol{\xi}(\mathbf{r}_1, \mathbf{r}_2) = \sum_{kl} d_{kl}\phi_k(\mathbf{r}_1)\phi_l(\mathbf{r}_2) \tag{16}$$

under the constraint that $d_{kl} = -d_{lk}$. The sum extends over the virtual space of orbitals.

10 One-particle orbital evaluation

We provide two major ways of evaluating the one-particle orbitals, the most expensive part of the QMC calculation. For a single electron, this is the problem of finding $\vec{m} = M_{orb}\vec{b}$, where $\vec{m}$ is a vector of the

values of each orbital, M_{orb} is the orbital coefficient matrix, and $\vec{b}$ is the vector of basis functions. The first (CUTOFF_MO) is a linear scaling technique, which, for localized orbitals and large enough systems, will take $O(N)$ time to evaluate all orbitals for all electrons. For each basis function, it creates a list of orbitals for which the coefficient is above a cutoff. This is done at the beginning of the calculation. Then, given an electron position, it loops over only the basis functions within range of the electron, and then only the orbitals contributed to by the basis function. These are both $O(1)$ cost for large enough systems, so all the orbitals for each electron is evaluated in $O(1)$ time, giving $O(N)$ scaling.

The second method (BLAS_MO) is slightly simpler. While it scales in principle as $O(N^2)$, it can be faster than CUTOFF_MO in medium-sized systems and certain types of computers that have very fast BLAS routines, such as Itaniums. Given an electron position, it loops through the basis functions within range of the electron, and adds to each molecular orbital the coefficient times the value of that basis function using fast BLAS routines.

11 Other Utilities

11.1 Conversion of One-particle Orbitals

Currently, QWalk can import and use the orbitals from GAMESS code (gaussian basis on molecules), CRYSTAL code (gaussian basis for extended systems), SIESTA code, and GP (plane waves for extended systems). The GP interface is not currently available for distribution due to licensing issues. More interfaces are planned, and are quite easy to add.

11.2 Plane Wave to LCAO converter

Gaussian basis sets have been used in quantum chemistry for years and have been developed to the point that there are well-defined sets which saturate the one-body Hilbert space surprisingly quickly. They are localized, which improves the scaling of QMC, and allow a very compact expression of the one-particle orbitals, so less basis functions need to be calculated. Overall, a gaussian representation can improve the performance of the QMC code by orders of magnitude over the plane-wave representation. We have developed a simple method to do this conversion that is fast and accurate. We start with the plane-wave representation of the k-th orbital $\Phi_k(\vec{r}) = \sum_{\vec{G}} c_{k\vec{G}} e_{\vec{G}}(\vec{r})$, and wish to find the LCAO equivalent $\Phi_k^{LCAO}(\vec{r}) = \sum_j a_{kj}\phi_j(\vec{r})$, where $e_{\vec{G}}$ is a plane-wave function and ϕ_j is a Gaussian function. Maximizing the overlap between Φ_k and Φ_k^{LCAO}, we obtain $Sa_k = Pc_k$, where $S_{ij} = \langle\phi_i|\phi_j\rangle$ and $P_{i\vec{G}} = \langle\phi_i|e_{\vec{G}}\rangle$. Then the Gaussian coefficients are given as $a_k = S^{-1}Pc_k$. All the overlap integrals are easily written in terms of two-center integrals for S, and P is easily evaluated in terms of a shifted Gaussian integral. The limiting part of the conversion is the calculation of the inverse of S, which can be done with fast LAPACK routines.

11.3 Summary on Qwalk.

QWalk is a significant step forward in creating a state of the art, usable, and extensible program for performing Quantum Monte Carlo calculations on electronic systems. It is able to handle very medium to large systems of electrons; the maximum size is mostly limited by the available computer time. It works in parallel very efficiently, so it can take advantage of large clusters, multi-core computers, etc. Since QWalk is available without charge and under the GNU Public license, it is hoped that it will help bring both development and use of Quantum Monte Carlo methods to a wide audience. More information such as testing examples, manual pages and other material is more convenient to obtain from the website www.qwalk.org.

12 Applications to transition metal oxides.

12.1 Transition metal oxides: strongly correlated materials.

Transition metal compounds and transition metal oxides (TMOs) in particular belong to the most complex and important types of solid materials. TMOs exhibit a multitude of collective effects such as ferro-, ferri- and anti-ferromagnetism, ferroelectricity, superconductivity, in addition to a host of structural transitions resulting from temperature and pressure changes or doping. In addition, several of these systems, such as FeO, can be identified as parent compounds of materials which are ecnountered in the Earth interior and therefore are of central interest for geophysics.

Electronic structure of TMOs poses a well-known challenge both for theory and experiment and this challenge has remained on a forefront of condensed matter research for decades. In particular, systems such as MnO, FeO, CoO, NiO and some other similar oxides have become paradigmatic examples of inuslators with strong electron-electron correlation effects and antiferromagnetic ordering. Let us for simplicty consider just the MnO solid for a moment. Since the transition elements in these systems have open d-shells, such solids should be nominally metals. However, for a long time it has been known and experiments have shown that these systems are *large gap insulators*. In addition, they exhibit antiferromagnetic ordering with the Neel temperatures of the order of a few hundred Kelvins. Interestingly, the gap remains present even at high temperatures when there is no long-range magnetic order. Using qualitative classification it was suggested that there are basically two relevant mechanisms: Mott-Hubbard and charge transfer. In the Mott-Hubbard picture, the gap opens because of large Coulomb repulsion associated with the double occupancy of the strongly localized d-states. The spin minority bands are pushed up in the energy, leading to gap opening. In the charge transfer mechanism, 4s electrons of the transition metal atom fill the unoccupied p-states of oxygen with resulting gap opening as well. In the real materials both of these mechanisms are present to a certain extent and therefore the systems exhibit insulating behavior. The antiferromagnetism happens on the top of this and is caused by weak super-exchange interactions between the moments of neighbouring transition metal atoms mediated by bridging oxygens. The localized d subshells feature unpaired spins which at low temperatures order into an antiferromagnetic AF II insulator with alternating spin (111) planes in cubic rocksalt structure. Due to magnetostrictive effects at low temperatures appear distortions of into a lower symmetry structures such as rhombohedral, for example, in the case of MnO and FeO.

It is also known that spin-unrestricted Hartree-Fock, surprisingly, provides a useful insight into the nature of the electronic structure in these systems. In particular, studies of MnO and NiO with unrestricted Hartree-Fock theory (UHF), seemingly a rather poor method choice, since it neglects the electron correlation completely showed some interesting results. The reason is that for transition elements the exchange, which is treated explicitly in the HF theories, is at least as important as correlation, especially for metallic ions with an effective $d-$subshells occupation close to half-filling. The UHF results confirmed the crucial role of exchange in TMOs and provided a complementary picture to DFT with overestimated gaps and underestimated cohesion, but also with the correct AF order, magnetic moments within 10% from experiments and reasonably accurate lattice constants. Moreover, unlike DFT approaches which predict insulator only for the AF II ground state, UHF keeps the gap open also for the ferromagnetic or any spin-disordered phases. This agrees with experiment which shows that MnO is an insulator well above the Néel temperature $T_N \sim 118$K since the spin ordering Mn-O-Mn superexchange mechanism is very weak and so that it enables localized moment flips without disturbing the overall gapped phase.

Here we present some results of our quantum Monte Carlo (QMC) calculations of MnO and also QMC calculations of FeO ambient and high pressure phases equations of state.

Our aim in using QMC for TMO has been to understand and quantify the impact of explicit treatment of both exact exchange and correlation on the key properties such as cohesion, band gap and several other properties.

MnO calculations. For the MnO solid we first carried out calculations with the spin-unrestricted Hartree-Fock and DFT (B3LYP and PW86) methods using the CRYSTAL98/03 packages. The orbitals were

expanded in gaussian basis sets with $(12s, 12p, 7d)$ gaussians contracted to $[3s, 3p, 2d]$ and $(8s, 8p, 1d)$ contracted to $[4s, 4p, 1d]$ for Mn and O atoms, respectively. Figure 1 shows the band structure of MnO solid which is obtained from UHF (a), B3LYP (b), PW86 (c) methods. Note that B3LYP hybrid functional contains 20% of the Hartree-Fock exchange so that it "interpolates" between the exact HF exchange and the effective local DFT exchange limits and it often provides an improved picture of excitations both in molecules and solids.

In QMC the MnO solid is represented by a supercell with periodic boundary conditions. This way of simulating an infinite solid involves finite size errors which scale as $1/N$ where N is the number of atoms in the supercell. The finite size errors affect mainly the estimation of cohesive energy where one needs to calculate the energy per primitive cell vs. isolated atoms. In order to filter out the finite size bias we have carried out VMC calculations of supercells with 8, 12, 16, 20 and 24 atom/supercell. Only Γ-point for each supercell and Ewald energies extrapolations were used to estimate the total energy in the thermodynamic limit. The most accurate and extensive fixed-node DMC (FN-DMC) calculations were carried out with B3LYP orbitals for 16 and 20 atoms in the supercell. The cohesive energy obtained by the DMC method shows an excellent agreement with experiment (Tab. 3). To evaluate the impact of the correlation on the gap we have estimated the energy of the $\Gamma \rightarrow$ B excitation by an exciton calculation. The QMC result for excitation energy is less perfect with the difference from experiment being a fraction of an eV. This clearly shows that the wavefunction and corresponding fixed-node error is larger for an excited state. Nevertheless, the differential energy gain for excited vs. ground state from correlation of

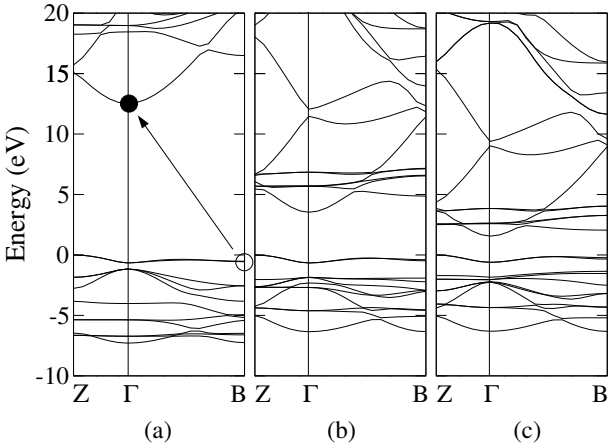

Figure 3: The band structures of MnO obtained by (a) the unrestricted Hartree-Fock method, (b) DFT/B3LYP functional, and (c) DFT/PW86 functional. The PW91 and PBE functionals provide essentially the same picture as the PW86 functional. The calculated excitation in QMC is indicated by an arrow on the UHF plot and the corresponding one-particle states are denoted by open and filled circles.

≈ 8 eV is substantial and demonstrates the importance of this effect both in qualitative and quantitative sense. Due to large computational demands, similar but statistically less precise DMC calculations were carried out also with the UHF orbitals. While for the ground state the difference between the two sets of orbitals was marginal, the excited state with UHF orbitals appeared higher in energy approximately by $\approx 1.5(0.5)$ eV indicating thus, not surprisingly, even larger fixed-node bias for the excited state in the UHF approach.

It is quite encouraging that the fixed-node DMC with the simplest possible single-determinant wavefunction leads to a consistent and parameter-free description of the basic properties of this strongly correlated system. An obvious question is whether one-determinant is sufficiently accurate for an antiferromagnet since the wavefunction with different spin-up and spin-down orbitals is manifestly not an eigenfunction of the square of the total spin operator. In order to eliminate the spin contamination one

Table 3: The MnO solid cohesive energy and B $\rightarrow \Gamma$ excitation energy calculated by UHF, DFT and DMC methods compared with experiment. The determinantal part of the DMC wavefunction used the B3LYP one-particle orbitals.

	UHF	PW86	B3LYP	DMC	Exp.
E_{coh}	6.03	11.00	9.21	9.40 (5)	9.50
B $\rightarrow \Gamma$	13.5	1.2	4.0	4.8 (2)	≈ 4.1

would need to explore wavefunction forms beyond the single-determinant Slater-Jastrow, for example, generalized valence bond wavefunctions. However, since the actual mechanism is the Mn-O-Mn superexchange, one can expect the resulting effect to be small and very difficult to detect within our error bars.

It is interesting to revisit now the one-particle results and provide some feedback from our QMC calculations. The analysis of orbitals indicates that the nature of the top valence bands is rather similar in all approaches with both p and d states having significant weights in these states across the Brillouin zone. This is supported also by the Mullikan population analysis which shows effective magnetic moments on Mn atoms in UHF, B3LYP and PW86/PW91/PBE methods to be 4.92, 4.84 and 4.78μ_B, respectively; these values are quite close to each other and border the range of experimental estimates of 4.58-4.78 μ_B.

The bottom of the conduction band is free-electron-like Γ state with significant amplitudes from atomic O(3s) and Mn(4s) orbitals and it is this state which is responsible for the DFT gap closing in ferromagnetic or spin-disordered phases. For the ferromagnetic phase B3LYP exhibits a gap of $\approx$ 2.4 eV and it is straightforward to check that by decreasing the weight of exact exchange the gap decreases. For example, with 10% of exact exchange in B3LYP the gap lowers to $\approx$ 1.2 eV. The functionals without the exact exchange, such as PW86/PW91/PBE, lead to ferromagnetic metals due to the overlaps with the uppermost valence bands and subsequent rehybridization of states around the Fermi level.

FeO calculations. If one applies mainstream DFT approaches to FeO, the results are highly unsatisfactory. First, the equilibrium atomic structure which comes out is not correct. Instead of the rocksalt antiferromagnet another structure, a tetrahedral distortion dubbed iB8, appears to have the lowest energy at equilibrium conditions. Interestingly, iB8 is actually a high pressure phase of FeO. This discrepancy is surprising since DFT methods typically lead to correct equilibrium structures and very reasonable geometric parameters such as lattice constants. Another problem appears in the electronic structure since for the correct structure and geometry DFT leads to a metallic state. More sophisticated methods beyond DFT have been applied to this system in order to reconcile some of the results with experiments, nevertheless, a number of questions remain unanswered. For example, at high pressures, FeO undergoes a structural transition into the iB8 phase, however, the value of the transition pressure which agrees with experiment is difficult to obtain using the mainstream approaches. Similar transition appears in MnO, where recent bechmarking of several DFT and post-DFT approaches provided transition pressure estimates between 65 and 220 GPa, i.e., more than 300% spread in the predictions. Significant discrepancies between expriments and DFT results exist also for CoO and more complicated transition metal compounds.

We have carried out QMC calculations of FeO using supercells with periodic boundary conditions to model the infinite solid. Several supercell sizes were calculated and k-point sampling of the Brillouin zone was carried out by the so-called twist averaging with the purpose of eliminating finite size effects. The core electrons were replaced by pseudopotentials for both Fe (Ne-core) and O (He-core). The largest simulated supercells had more than 300 valence electrons and the total energies were sizeable due to the presence of "semicore" 3s and 3p states of Fe in the valence space, what have made the calculations rather demanding. The wave function had the Slater-Jastrow form and the orbitals were obtained from unrestricted (spin-polarized) calculations within DFT with hybrid functionals and HF.

In Tab. 4 are shown the QMC calculated equilibrium parameters. Note that QMC identifies the correct

Table 4: Comparision of the calculated structural properies of FeO solid in DFT and in the fixed-node DMC with experimental data. The energy difference E_{iB8}-E_{B1} is evaluated at the experimental lattice constant 4.334 Å.

Method/quantity	DFT/PBE	FN-DMC	Exper.
E_{iB8}-E_{B1} [eV]	-0.2	0.5(1)	> 0
cohesion energy [eV]	~ 11	9.66(4)	9.7
lattice constant [Å]	4.28	4.324(6)	4.334
bulk modulus [GPa]	180	170(10)	~ 180
band gap [eV]	~ 0	2.8(3)	2.4

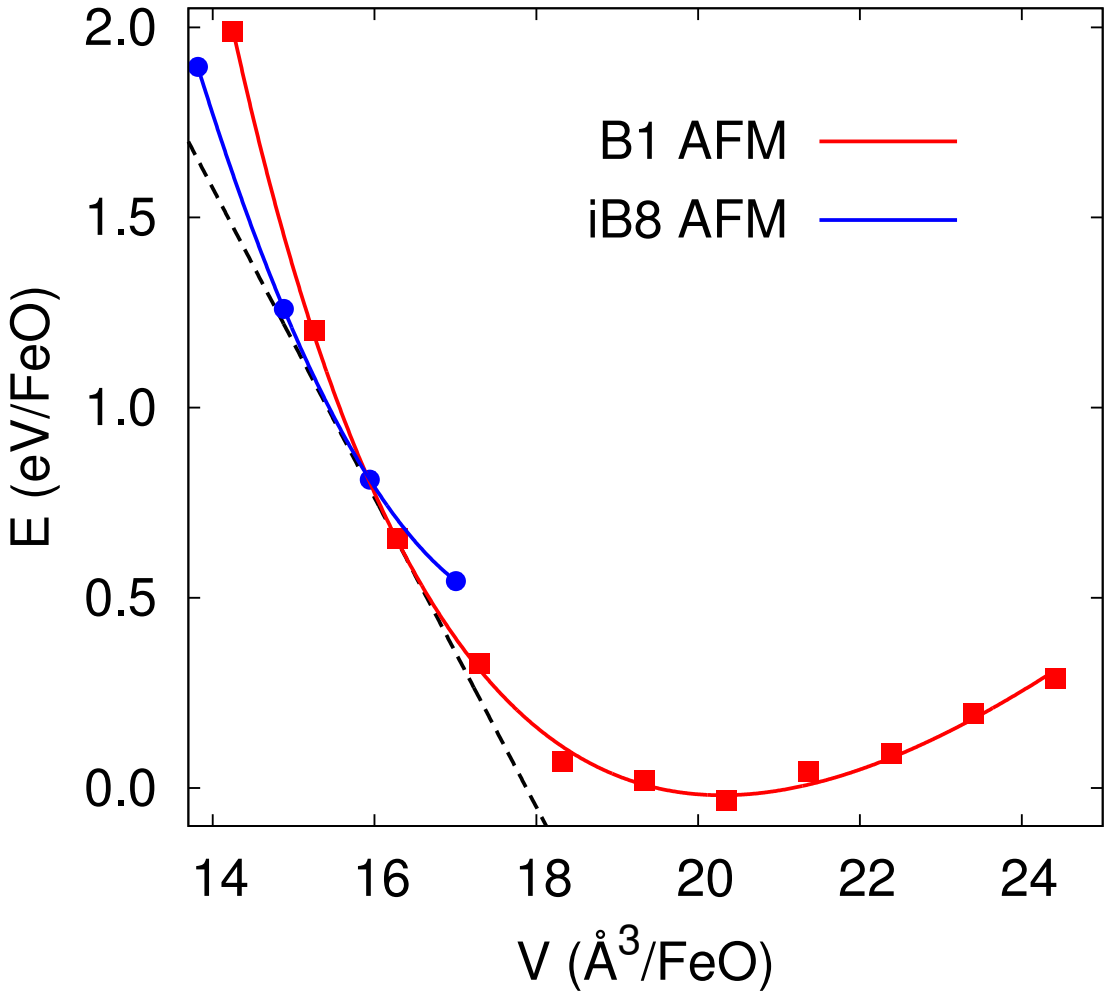

Figure 4: FN-DMC Energy as a function of volume for FeO for B1 (red squares) and iB8 (blue circles) phases. Lines are fits with Murnagham equation of state.

equilibrium structure and provides very accurate value of the cohesive energy. Cohesive energies are very difficult to calculate since the DFT methods show typical bias of 15-30%. At present, there is basically no other method besides QMC which can get this level of accuracy. Note also good agreement with experiments for the other quantities including the band gap. In QMC the band gap is calculated as a

difference of two total energies— ground state and excited state, where the excited state is formed by promoting an electron from the top valence band into the conduction band.

In addition, the equations of state have been calculated for both the equilibrium structure and also for the high pressure phase, see Fig. 4. The estimated transition pressure is 65(5) GPa, at the lower end of the experimental range 70-100 GPa. Clearly, the agreement with exepriment is not perfect and reflects several idealizations used in our calculations. We checked that the rhobohedral distortion did not change the results within our error bars so it appears unlikely that this was the dominant contribution. The fact that the experimental results also vary significantly suggests that there other reasons need to be considered. For example, it is well known that FeO is basically always slightly nonstochiometric what could affect the experimental pressures significantly. Another reason could defects which could also push the experimental observations towards higher pressures. Clearly, this question will have to be resolved with further effort on both theoretical and experimental fronts.

The calculations clearly illustrate the capabilities of QMC methods and considering that only the simplest trial wave function of Slater-Jastrow type was employed, the results are remarkable and very encouraging. Note that the calculations do not have any free non-variational parameters. It is simply the best possible solution within the trial function nodes and the given Hamiltonian.

More information about these projects can be found in Refs. [3],[9],[12] at the beginning of this report. We note that **our study of FeO solid was the first QMC calculation of transition metal oxides at high pressures** and provided a convincing demonstration of the QMC method potential for this important class of solid materials.